metals

MDPI

Review

Selective Adsorption and Recovery for Low-Quality Lithium-Containing Resources: Materials, Mechanism, and Outlook

Xiaofei Meng [1], Haitao Zhou [1,2,*], Xiaoping Zou [1], Yingping Jiang [1], Shengmei Zhang [1], Yanwen Sun [1] and Chi Zhang [1,*]

[1] Technical Center for Pyrometallurgy, BGRIMM Engineering Technology Co., Ltd., BGRIMM Technology Group Co., Ltd., Beijing 100160, China; mengxiaofei@bgrimm.com (X.M.); zou_xiaoping@bgrimm.com (X.Z.); jyp@bgrimm.com (Y.J.); zhangshengmei@bgrimm.com (S.Z.); sunyanwen@bgrimm.com (Y.S.)
[2] School of Metallurgical and Ecological Engineering, University of Science and Technology Beijing, Beijing 100083, China
* Correspondence: zhouhaitao@bgrimm.com (H.Z.); zhang_chi@bgrimm.com (C.Z.)

Abstract

With the rapid expansion of the global lithium-battery industry, efficient and sustainable lithium recovery from low-grade lithium resources, such as lithium precipitation mother liquor characterized by a high sodium-to-lithium ratio, has become a critical research challenge. Among the emerging technologies, the adsorption method, recognized for its operational simplicity, high selectivity, and process flexibility, has garnered significant attention. This review systematically summarizes recent advancements in two primary categories of adsorbents for selective lithium recovery: organic adsorbents (crown ether-based materials) and inorganic adsorbents (aluminum-based layered double hydroxides (LiAl-LDHs), titanium-based ion sieves (H_2TiO_3, $H_4Ti_5O_{12}$), and manganese-based ion sieves (HMn_2O_4, $H_{1.6}Mn_{1.6}O_4$, $H_4Mn_5O_{12}$). For each class, the synthesis methods, adsorption mechanisms, performance (capacity, selectivity, kinetics, and cycling stability), and key influencing factors are thoroughly discussed and compared. Titanium-based sieves demonstrate high capacity and stability, manganese-based materials show excellent kinetics, aluminum-based adsorbents offer industrial scalability, and crown ether-based materials exhibit superior ion size selectivity. The review also identifies limitations, such as the slow kinetics of H_2TiO_3, manganese dissolution in manganese-based ion sieves, and the cost of functionalized organics. Finally, future research directions are proposed, focusing on enhancing adsorption kinetics and stability via material design (e.g., morphology control, doping, hybridization), developing scalable and cost-effective synthesis routes, and exploring the integration of adsorption with other separation technologies to create efficient hybrid processes for the sustainable exploitation of low-grade lithium.

Keywords: low-quality; lithium recovery; adsorption materials; organic and inorganic; manganese-based ion sieves; titanium-based ion sieves

Check for updates

Academic Editor: Mark E. Schlesinger

Received: 30 June 2026
Revised: 26 July 2026
Accepted: 4 August 2026
Published: 12 August 2026

Copyright: © 2026 by the authors. Licensee MDPI, Basel, Switzerland. This article is an open access article distributed under the terms and conditions of the Creative Commons Attribution (CC BY) license.

1. Introduction

Energy is one of the key influencing factors for national development and human lifestyles. Driven by population growth and technological advancements, global energy demand has increased sharply. The drawbacks of traditional non-renewable energy sources have become more evident. Green energy is more in line with the contemporary era's development [1,2]. Energy storage systems for renewable sources such as wind power, hydropower, and solar energy, as well as electric vehicles, all require the participation of lithium-ion batteries, which has also increased the demand for lithium resources [3,4].

Lithium resources are mainly stored in lithium-bearing ores and salt-lake brines. As a major consumer of lithium resources, China has long relied on imports to meet its domestic lithium demand [5,6]. Reducing the reliance on imported lithium resources can play a positive role in promoting the construction of new energy and achieving the nation's "carbon neutrality" goals.

Secondary lithium-bearing resources, such as lithium-containing mother liquor produced during lithium extraction and refining processes [7], seawater [8], geothermal water, and oilfield brine as a byproduct of oil and gas extraction [9,10], typically contain measurable amounts of lithium. However, the lithium concentration is generally low, along with a high content of impurity ions, such as sodium. Table 1 summarizes the lithium contents in typical low-grade lithium resources, including lithium-containing mother liquor, geothermal water, and others. The efficient and sustainable utilization of such low-grade lithium resources has become a research focus and a technical challenge. Conventional methods often adopt evaporation and crystallization, which remove most of the water to concentrate Li^+ before precipitation [11]. A key drawback of these traditional approaches is the generation of secondary lithium-containing wastewater during the reprecipitation step, primarily due to the solubility limit of Li_2CO_3. Moreover, the final product may carry impurities, leading to reduced lithium recovery efficiency and deteriorated product quality. Additionally, traditional lithium extraction technologies are time-consuming and not considered viable for long-term application [12,13].

Table 1. The lithium content in typical low-grade lithium resources.

Lithium-Containing Resources	Li^+ ($g \cdot L^{-1}$)	Na^+ ($g \cdot L^{-1}$)	Mg^{2+} ($g \cdot L^{-1}$)	Ref.
Lithium-containing mother liquor	1.42	55.62	/	[7]
Seawater	0.178	10.8	1.29	[8]
Salton Sea Geothermal	0.09–0.44	/	/	[9]
Eagle Ford Oilfield Brine source	0.0725	51.55		[9]

In recent years, methods for enhancing lithium recovery and product quality have emerged, mainly including adsorption, solvent extraction, and nanofiltration membrane separation [10,14–20]. Over the past two decades, the number of publications on lithium extraction from various salt-lake brines has increased significantly. Since 2020, lithium recovery from low-grade solutions such as lithium-containing mother liquor has attracted growing attention. The adsorption method has become a research hotspot due to its advantages of simple operation, wide applicability, and high selectivity [21,22]. The adsorption method relies on the selection or design of adsorbent materials with Li^+-recognition capability, which realize selective separation and recovery of lithium ions via specific physical or chemical interactions [23]. Adsorbent materials constitute the core of the adsorption process. Ideally, an adsorbent should exhibit high selectivity, stability, and sufficient adsorption capacity [24–26]. These properties enables the material to capture as much Li^+ as possible per unit mass, ensuring selective separation of Li^+ from complex, high-salinity solutions while maintaining excellent structural and mechanical stability during repeated adsorption-desorption cycles.

Unlike previous general reviews focusing on salt-lakes resources, the present review specifically addresses low-grade lithium resources with ultra-high Na/Li ratios, particularly lithium precipitation mother liquor. This review discusses the adsorption mechanisms, applicability, advantages, and limitations of organic and inorganic adsorbent materials, filling the gap in the systematic analysis of such low-grade lithium-bearing solution systems in the existing literature. Finally, based on the current research status, future development directions for the treatment of low-grade lithium-containing solutions are prospected, and potential optimization strategies are proposed. This work proposes future development

trends emphasizing hybrid processes integrating adsorption with other separation units, offering a practical industrial roadmap.

2. Adsorption Method

Adsorption represents a highly selective, operationally simple, good reusability, widely applicable, and process-flexible low-cost technology for the selective separation of target metals from aqueous solutions [27–30]. At present, commonly used adsorption materials including organic and inorganic adsorption materials [31]. Organic adsorbents are mainly represented by crown ethers, porphyrin-based organic polymers, and cation exchange resins [32,33]. Inorganic adsorbents mainly include aluminum-based adsorbents, lithium ion filters, and carbon-based materials [24,34,35]. This paper reviews relevant studies on different adsorbents, compares the preparation methods, separation effects, and separation mechanisms of these adsorbents and analyzes their respective applicability, so as to provide a theoretical basis for the recovery and recycling of lithium resources in low-grade lithium solutions.

2.1. Organic Adsorption Materials

The selectivity of ether-based adsorbents toward specific ions primarily depends on the matching between their cavity size and the target ions radius [36]. The oxygen atoms within ether groups donate lone-pair electrons, enabling stable coordination with metal ions. When the diameter of the target ion is close to the cavity size of the crown ether, the ion can readily enter the cavity and become bind (Figure 1). Research indicates that 12- to 14-membered crown ethers exhibit a stronger affinity for Li^+ [37,38]. For instance, the cavity diameter of crown ethers (e.g., 12-crown-4, 14-crown-4) or their derivatives generally ranges from 0.122 to 0.153 nm, while the diameter of lithium ions (Li^+) is approximately 0.136 nm. This close dimensional match allows Li^+ to effectively embed into the cavity and form strong electrostatic interactions with the oxygen atoms of the ether groups, thereby achieving selective capture. In contrast, ions such as Na^+ (0.205 nm), K^+ (0.275 nm), and Cs^+ (0.341 nm) have diameters significantly larger than the cavity size of such crown ethers, making it difficult for them to form stable coordination structures [36]. In practical extraction processes, the crown ether (in the organic phase) complexes with Li^+ at the aqueous-organic interface to form a cationic complex. Simultaneously, hydrophobic anions acts as counter-anions and associate with this complex, forming an electrically neutral, hydrophobic ion pair. This final step enables the efficient and selective transfer of lithium from the aqueous phase into the organic phase, for separation and enrichment. Torrejos et al. [39] synthesized a series of dihydroxy crown ethers via the intermolecular cyclization of diepoxides and dihydroxybenzenes and applied them for lithium separation. The results demonstrated that these crown ethers exhibit high selectivity for lithium due to their ideal cavity size matching with Li^+, with the lithium–sodium separation coefficient reaching up to 2514. However, liquid–liquid extraction has a drawback: harmful solvents are prone to leakage [40]. To avoid this issue, crown ether organic adsorbents are typically immobilized on inorganic supports and polymers [41,42]. These support materials should feature advantages such as high mechanical strength, excellent stability, and ease of functional modification. Xu et al. [43] adopted hierarchically porous silica (HPS) prepared by a dual-template method as a carrier, and prepared an adsorbent via chemical grafting. This material features a rod-like nanostructure and a bimodal mesopore distribution. The adsorption behavior for Li^+ conforms to the Langmuir isotherm and pseudo-second-order kinetics model, achieving a maximum adsorption efficiency of 94.34%. After five adsorption–desorption cycles, it retains 90.7% of its initial adsorption capacity. Nisola et al. [40] realized in situ growth of Fe_3O_4 nanoclusters on the surface of graphene

oxide (GO), followed by grafting ethynylbenzene linkings to fabricate composite adsorbent. Among these, the 12CE4@Fe_3O_4-rGO composite exhibits extremely high selectivity for Li^+, with selectivity coefficients (α) for Na^+, K^+, Mg^{2+}, and Ca^{2+} ranging between 367 and 14,513. The crown ether utilization rate approaches 100%, with a loading capacity of 1.03 mmol·g^{-1}, and it possesses good water dispersibility, magnetic recoverability, and cycling stability.

Apart from the cavity-size effects, the type and quantity of substituents on the ring of the chelating atoms in the crown ether also have certain exert considerable influences on lithium extraction [44–49]. Wu et al. [33] synthesized a high-molecular-weight composite 2H12C4-D113 bearing crown ether moieties at a resin-to-p-toluene sulfonic acid mass ratio of 1:0.5 and a temperature of 110 °C, and applied it to extract lithium ions (Li^+) from the low-grade lithium-bearing solution obtained from the desiliconization liquor of coal-based solid waste. The solution was characterized by a high Na^+/Li^+ ratio, with Li^+ and Na^+ concentrations of 0.27 g·L^{-1} and 101 g·L^{-1}, respectively. The results demonstrated that 2H12C4-D113 exhibited remarkable Li^+ selectivity and adsorption capacity in both neutral and alkaline environments. Specifically, the Li^+ adsorption capacity of 2H12C4-D113 reached 10.12 mg·g^{-1} under neutral conditions, which was 4.05 times higher than that of the non-functionalized material. Furthermore, the adsorption capacity was further enhanced to 21.38 mg·g^{-1} in the alkaline system. Yang et al. [50] grafted diamino-dibenzo-14-crown-4 ether (DAB) onto 14-crown-4 polyimide (14C4PI) via a nucleophilic substitution reaction, and fabricated a nanofiber membrane using a electrospinning technology. Through the optimization of the DAB addition amount and reaction time, the crown ether loading capacity increased from 1.38 mmol·g^{-1} to 2.27 mmol·g^{-1}, with a grafting efficiency of 83.4%. The equilibrium adsorption capacity for Li^+ improved from 40.17 mg·g^{-1} to 60.71 mg·g^{-1}. The adsorption process follows pseudo-second-order kinetics and the Langmuir model. The separation factors for Li^+ relative to Na^+, K^+, Mg^{2+}, and Ca^{2+} are 69.24, 79.4, 37.46, and 67.53, respectively [50]. Torrejos [36] reported that the crown ether with carboxyl side arms significantly enhanced the lithium adsorption capacity under pH $\geq$ 7 conditions. The adsorption process conformed to the Langmuir model, and in competitive adsorption, it revealed a selectivity sequence of $Li^+ > Na^+ > Mg^{2+} > Ca^{2+} > K^+ \approx Sr^{2+}$. Huang et al. [51] integrated surface ion-imprinting with magnetic separation technology to fabricate a magnetic crown ether-imprinted polymer. Leveraging the specific recognition of Li^+ by hydroxyl-modified crown ether, the separation selectivity coefficients for Li^+/Na^+, Li^+/K^+, and Li^+/Mg^{2+} are 7.74, 2.75, and 2.98, respectively. Furthermore, its magnetic properties enable rapid separation under an external magnetic field, eliminating the need for traditional centrifugation and filtration steps and significantly improving operational efficiency. Zhu et al. [52] found that a novel crown ether-based polyimide membrane material was synthesized via the polycondensation of di(aminobenzo)-14-crown-4 with 4,4′-(hexafluoroisopropylidene)diphthalic anhydride. The adsorption of Li^+ onto this membrane conforms to pseudo-second-order kinetics and the Langmuir model. The separation factors for Na^+, K^+, Mg^{2+}, and Ca^{2+} are 45.6, 48.3, 23.5, and 41.2, respectively. Density-functional-theory calculations agree well with experimental results, and the material exhibits good stability. Its performance advantages are attributed to the synergistic sieve-chelating effect of the crown ether and its porous structure. Although most experimental results indicate that crown ether-based organic adsorbents exhibit excellent adsorption performance and selectivity (Table 2), their current industrialization level remains relatively low. This is primarily due to the complex synthesis process and high cost, coupled with the fact that the lithium ion complexation capability of the monomers is influenced by multiple factors. Reducing their manufacturing costs would significantly enhance their competitiveness for market-oriented applications.

Table 2. Performance of crown ether ligand composite adsorption materials.

Crown Ether Ligands	Li^+ Concentration ($mg \cdot L^{-1}$)	pH	Adsorption Capacity ($mg \cdot g^{-1}$)	Selectivity α(Li/Na)	Ref.
2-hydroxymethyl-12-crown-4	200	13	58.71	12.4	[33]
2-methylol-12-crown-4	17,920	5	1.85	25.46	[43]
14-crown-4 polyimide	400	7	60.71	69.24	[50]
Dibenzo-14-crown-4	18.82	6	0.28	7.74	[51]
dibenzo-14-crown-4	400	7	34.05	45.6	[52]

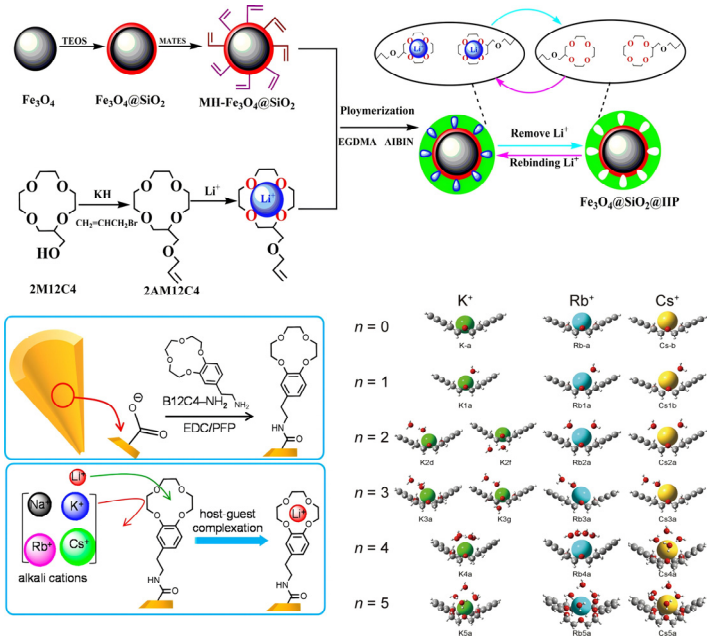


Figure 1. Selective lithium separation enabled by cavity size matching in host–guest chemistry (adapted from [53–55]).

2.2. Aluminum-Based Adsorbents

Aluminum-based adsorbents are developed from aluminum salt adsorbents. The basic framework of these adsorbents is mainly composed of aluminum hydroxide. It is currently the only type of adsorbent material that has been put into industrial application. The most widely adopted form is lithium aluminum layered double hydroxide adsorbent, which is formed by the orderly assembly of positively charged layers and interlayer anions into stacks [56]. Their structural foundation is analogous to typical layered hydroxides, such as gibbsite ($Al(OH)_3$), consisting of alternating stacks of metal hydroxide main layers and anion interlayers, forming an extended two-dimensional framework. In this structure, the partial isomorphous substitution of divalent cations by trivalent aluminum ions results in positively charged host layers. Charge balance is maintained by anions (e.g., Cl^-) residing in the interlayer region. Metal cations are located at the centers of edge-sharing [MO_6] octahedral units, which are interconnected via hydroxyl groups at shared vertices, constituting continuous two-dimensional sheets. The interlayer domain contains water molecules partially bound through hydrogen bonding. Li/Al-LDHs are stabilized overall by a combination of interlayer electrostatic interactions, hydrogen bonds, and van der Waals forces (Figure 2). Their chemical composition can be represented by the general formula $[Li_mAl_2(OH)6]Clm \cdot nH_2O$, where m ranges from 0 to 1 [56–59].

The adsorption and desorption processes of lithium by the aluminum-based adsorbent can be described by the following reaction Equation (1).

$$xLiCl + (1 - x)LiCl \cdot mAl(OH)_3 + (n + 1)H_2O \rightleftarrows LiCl \cdot mAl(OH)_3 \cdot nH_2O + H_2O \quad (1)$$

The adsorption of Li^+ on Li/Al-LDHs follows the pseudo-second-order kinetic model, suggesting that the rate-determining step is chemisorption—specifically, ion exchange between interlayer species and Li^+—rather than a process governed solely by external film diffusion or bulk Li^+ concentration. Further analysis of the mass transfer mechanism of zinc-doped Li/Al-LDHs using the Weber–Morris intraparticle diffusion model revealed that the adsorption process comprises three consecutive stages:

(1) External liquid-film diffusion stage—lithium ions diffuse from the bulk solution across the liquid-film boundary layer to the surface of the adsorbent particles;

(2) Intraparticle diffusion via mesopores—lithium ions migrate along the internal mesoporous channels of the material toward the active sites;

(3) Lattice consolidation stage—lithium ions are ultimately embedded into the octahedral vacancies within the crystal structure, finalizing the chemisorption immobilization.

After lithium ions traverse the diffusion barriers formed by membranes and pores, the adsorption process commences. Assisted by the combined effects of van der Waals forces and electrostatic attraction, lithium ions become anchored to the active sites of the material, forming a uniform monomolecular adsorption layer of hydrated lithium ions. This process triggers a microscopic reaction mechanism comprising three steps:

(1) Dissociation of the Hydration Shell: The hexagonal cavities formed by adjacent $Al(OH)_3$ units contain triangular oxygen windows with specific dimensions (O–O distances of 2.75–3.45 Å), which selectively recognize lithium ions. Although these pore sizes are larger than the effective diameter of hydrated lithium ions (approximately 1.36 Å), they are smaller than the ionic diameter of fully desolvated lithium ions. This size mismatch forces lithium ions to undergo desolvation, shedding their hydration shell.

(2) Lattice Penetration and Local Structural Reconstruction: In the initial stage, electrostatic repulsion and steric hindrance from interlayer –OH groups impede further entry of lithium ions. As lithium ions approach the oxygen windows, mutual repulsion between protons induces localized displacement of –OH groups, creating transient diffusion channels that allow lithium ions to pass through.

(3) Octahedral Site Occupation and Structural Relaxation: Lithium ions that successfully traverse the triangular windows embed into the Al–O_6 octahedral vacancies. This prompts surrounding –OH groups to rotate and adjust their positions, alleviating electrostatic repulsion between protons and lithium ions and achieving structural stabilization.

During this process, the migrating lithium ions undergo an exchange reaction with hydrogen ions in the crystal lattice. This exchange not only disrupts the original charge balance of the host material and weakens the interlayer hydrogen bonding but also further induces the intercalation of anions to restore electroneutrality in the system, thereby facilitating the entry of more lithium ions into octahedral coordination sites. When the concentration of lithium ions in the system decreases, the desorption process occurs in reverse: lithium ions are released from the layered framework and diffuse into the solution phase. Simultaneously, anions and water molecules undergo coordinated migration to maintain charge conservation throughout the system. Thus, throughout the dynamic cycle of adsorption and desorption, anions consistently play a critical role in modulating and stabilizing the charge state.

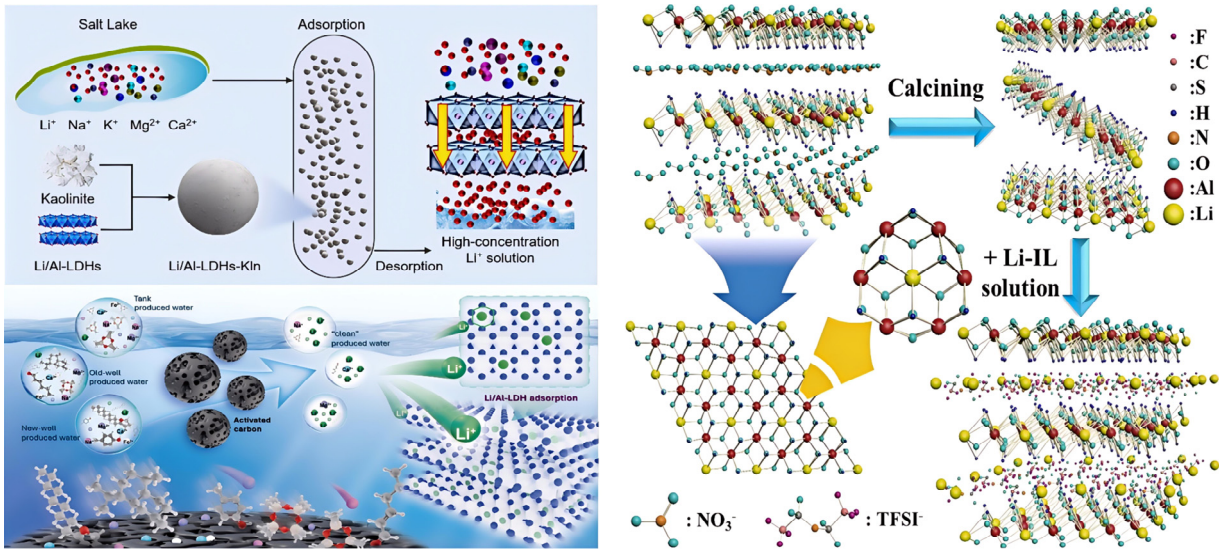


Figure 2. Adsorption mechanism of lithium–aluminum layered double hydroxide (Li/Al-LDH) (adapted from [60–62]).

The preparation methods of aluminum-based adsorbents mainly include the immersion method, precipitation method, and mechanical activation method. Luo et al. [63] synthesized an aluminum-based adsorbent via a hydrothermal method using $Al_2(SO_4)_3 \cdot 18H_2O$ and urea as raw materials. They hydrothermally obtained a porous powder precursor composed of $NH_4Al_3(SO_4)_2(OH)_6$ and γ-AlOOH, followed by lithiation with a LiOH aqueous solution to yield a mixed porous powder of Li-Al-LDHs containing $NH_4Al_3(SO_4)_2(OH)_6$ and $Li_2Al_4(OH)_{12}SO_4 \cdot xH_2O$. The powder was further processed into granular form using sodium alginate. The resulting adsorbent exhibited a maximum lithium adsorption capacity of 9.66 $mg \cdot g^{-1}$, along with good recyclability, demonstrating potential for industrial-scale application. Zhang et al. [64] prepared a Li–Al–OH layered double hydroxide via a mechano-hydrothermal route. The process involved dry ball-milling of $Al(OH)_3$ for 1 h, followed by hydrothermal lithiation with a $LiOH \cdot H_2O$ solution, yielding a highly crystalline and well-dispersed Li–Al–OH layered double hydroxide. This synthesis method is simple, feasible, and environmentally friendly with low energy consumption. Qin et al. [65] prepared magnetic aluminum-based adsorbents (MLDHs) by coprecipitation for the separation of lithium ions from aqueous solutions, which achieved a lithium ion adsorption capacity of 8.22 $mg \cdot g^{-1}$ under static adsorption conditions. This material demonstrated good selectivity in multi-ion coexistence solutions, with its adsorption behavior conforming to the pseudo-second-order kinetic model and the Langmuir isotherm adsorption model. Thermodynamic analysis indicated that the adsorption process is spontaneous and endothermic. Zhang et al. [66] developed a lithium–aluminum layered double hydroxide material with a regular two-dimensional hexagonal layered structure through a simple coprecipitation method, achieving an adsorption capacity of 7.27 $mg \cdot g^{-1}$ at room temperature. The material's selectivity order for different ions is $Li^+ > Na^+ > K^+ > Ca^{2+} \gg Mg^{2+}$, and it maintained stable adsorption performance after 12 adsorption–desorption cycles. Wu et al. [67] developed an aluminum-based lithium adsorbent that exhibited an adsorption capacity of 7.44 $mg \cdot g^{-1}$ under conditions of 30 °C and a lithium concentration of 500 mg/L. After seven cycles, the capacity retention rate reached 96.18%. The ion selectivity order of this material is $Li^+ > Mg^{2+} > Na^+ > K^+ > Ca^{2+}$, demonstrating excellent cycling stability. Most of the studies mentioned above have demonstrated that aluminum-based adsorbents exhibit excellent stability and cycling performance (Table 3). However, compared with other adsorbents, such as titanium-based ion sieves, manganese-based ion sieves, and crown

ether-based organic adsorbents, their relatively low adsorption capacity and selectivity remain the main factors limiting their large-scale industrial application.

Table 3. Adsorption performance of aluminum-based composite adsorption materials.

Adsorbent	Li^+ Concentration ($mg \cdot L^{-1}$)	pH	Adsorption Capacity ($mg \cdot g^{-1}$)	Selectivity α(Li/Na)	Ref.
MLDHs	412	9	8.22	23.52	[65]
Li/Al-LDHs	399	8	7.27	21.79	[66]
Al/Li-LDHs	500	7	9.12	154.47	[67]
Fe-Li/Al-LDHs	549	10	9.46	/	[68]
LDHs	400	7.5	10.4	236.7	[69]
Li-Al-CO_3 LDH	400.2	14	14.68	972.11	[70]

2.3. Ion Sieve Adsorbents

Ion sieve adsorbents exhibit effective ion recognition and size-sieving capabilities for extracting specific metal ions. This mechanism enables ion sieves to selectively extract lithium over other alkaline earth metals [71]. Lithium ion sieves comprise a series of adsorbents with distinctive chemical structures, allowing for the insertion of target ions into inorganic compounds. Precursors of lithium ion sieves are synthesized via methods such as hydrothermal treatment or high-temperature solid-state reactions. Subsequently, the target ions are eluted from the precursors using eluents. After delithiation, the resulting compounds maintain well-defined vacancy structures without structural collapse. These vacancy-containing compounds demonstrate reliable sieving and memory effects towards the reintroduced target Li^+, permitting only Li^+ to occupy the vacancies, thereby enabling the selective adsorption of Li^+ from multi-ion coexistence systems [25,71,72]. Lithium ion sieves are generally categorized into two main types: lithium titanium oxides and lithium manganese oxides [73–75].

2.3.1. Titanium-Based Ion Sieves

Titanium-based ion sieves (TIS) have emerged as a highly promising class of adsorbents for selective lithium recovery, primarily due to their robust Ti–O bonds, exceptional 2 structural stability, remarkable 5 acid resistance, and outstanding lithium adsorption performance (Table 4). The parent lithium titanate (LTO) structures are predominantly categorized into two crystalline architectures: layered Li_2TiO_3 and spinel-type $Li_4Ti_5O_{12}$.

The chemical formula of layered LTO can be expressed as $Li[Li_{1/3}Ti_{2/3}]O_2$. Its crystal structure consists of alternating layers of lithium and lithium–titanium ($LiTi_2$) layers, with the lithium layers accounting for 75% of the total lithium atoms. Oxygen atoms adopt in a cubic close-packed arrangement, while the metal atoms occupy the octahedral interstitial sites [73] (Figure 3). The adsorption mechanism of HTO, derived from LTO via acid treatment, primarily relies on an ion exchange process, rooted in the structural memory effect of the ion sieve (Figure 3). Upon elution with acid, vacancies matching the size of lithium ions are left behind. These vacancies preferentially re-occupy Li^+ from aqueous solutions, while the spatial effect of these vacancies excludes other ions with different radii (such as magnesium, calcium, sodium, and others), thereby achieving selective adsorption of lithium ions. The material can be regenerated through proton exchange. However, it is critical to note that effective ion exchange mainly occurs in the lithium layers, as the activity of Li^+ in these layers is lower than that of Li^+ in the ($LiTi_2$) layers. In the protonated product $H[H_{1/3}Ti_{2/3}]O_2$, the H^+ in the (HTi_2) layers cannot exchange with Li^+, as shown in Equation (2). Consequently, although HTO demonstrates high selectivity, its practical adsorption capacity invariably is always lower than its theoretical value.

$$xLiCl + (1 - x)LiCl \cdot mAl(OH)_3 + (n + 1)H_2O \rightleftarrows LiCl \cdot mAl(OH)_3 \cdot nH_2O + H_2O \quad (2)$$

Chitrakar et al. [72] demonstrated that at pH = 6.5, the Li^+ adsorption capacity reached 32.6 $mg \cdot g^{-1}$, with separation coefficients between Li^+ and other competing ions all exceeding 100, confirming the high ion selectivity of H_2TiO_3. Nevertheless, the high structural stability of H_2TiO_3 leads to relatively sluggish adsorption kinetics, typically requiring up to one day to reach adsorption equilibrium. Additionally, the layered Li_2TiO_3 crystal structure is prone to rearrangement, which reduces its adsorption capacity. To overcome these bottlenecks, recent research has emphasized the synthesis of high-quality LTO precursors and morphology optimization [76–81]. Gu et al. [82] developed an innovative approach utilizing $C_2H_3LiO_2 \cdot 2H_2O$ as a lithium source Li_2CO_3 to synthesize LTO materials. The resulting adsorbent followed Langmuir and pseudo-second-order models, exhibiting an exceptional Li^+/Na^+ separation factor (α = 3414.69). Subsequent studies by Li et al. [83], systematic investigation of different TiO_2 precursor phases (amorphous, anatase, rutile) revealed their significant impact on H_2TiO_3 adsorption properties. Contact angle measurements established a clear correlation between material hydrophilicity and adsorption performance. Among three HTO variants, anatase-derived HTO-400 exhibited superior lithium adsorption due to optimal hydrophilicity, achieving 34.2 mg/g equilibrium capacity within 24 h with Li^+/Na^+ separation factor α = 19.96. Zhang et al. [79] used $LiOH \cdot H_2O$ and TiO_2 precursors, and Li_2TiO_3 was synthesized and converted to H_2TiO_3 adsorbent. Crystal-phase effects on Li^+ extraction and adsorption performance were thoroughly examined. The results demonstrated that the anatase structure significantly enhanced both Li^+ extraction (98.69% maximum) and adsorption capacity (39.2 $mg \cdot g^{-1}$ maximum) compared to rutile. Solution parameters including pH, solid/liquid ratio, temperature, and concentration profoundly influenced adsorption characteristics [84]. Optimized conditions effectively mitigated H^+ accumulation limitations. The process adhered to Langmuir and pseudo-second-order models, with thermodynamic parameters confirming feasibility, spontaneity, and endothermic nature. H_2TiO_3 exhibited remarkable stability and recyclability, achieving record capacity (94.5 $mg \cdot g^{-1}$) with Li^+/Na^+ separation factor α = 705.3.

In addition to layered structures, spinel titanium oxides derived from spinel-type $Li_4Ti_5O_{12}$ precursors constitute a class of titanium-based ion sieves that exhibit substantial lithium adsorption capacity and favorable cycling stability [85–93]. Moazeni et al. [85] synthesized spinel $Li_4Ti_5O_{12}$ with a nanotubular structure, featuring diameters of 50–70 nm and lengths of 1–2 μm, via a two-step low-temperature hydrothermal reaction. The as-prepared material exhibited a lithium adsorption capacity of 39.43 $mg \cdot g^{-1}$ in a lithium-containing solution with an initial Li^+ concentration of 120 $mg \cdot L^{-1}$. $H_4Ti_5O_{12}$ nanofiber lithium ion sieves, demonstrating excellent Li^+ adsorption performance and high selectivity, were synthesized by Wei et al. [86] via a combined electrospinning and calcination method. The obtained adsorbent achieved a notable lithium adsorption capacity of 59.1 $mg \cdot g^{-1}$, closely approaching its theoretical value of 63.77 $mg \cdot g^{-1}$. Despite the structural stability, strong Ti–O bonds, and superior acid resistance of $Li_4Ti_5O_{12}$, the presence of rutile TiO_2 and Li_2TiO_3 phases, which commonly occur during synthesis [87], significantly compromises its structural integrity and adsorption capacity. A comparative study of $H_4Ti_5O_{12}$ adsorbents (HTO-OS and HTO-NS) revealed HTO-NS superiority with 35.5 $mg \cdot g^{-1}$ capacity and <2 h equilibrium time, attributed to distinct dehydration processes and exposed facets. Mechanism analysis identified hydrated Li^+ dehydration followed by ion exchange as the primary adsorption pathway [94].

To further enhance performance, several advanced strategies have been explored. Fe-Zr co-doping modulated LIS surface properties and internal structure. Successful incorporation increased 8a site Li-O bond length and O^{2-} content. HTFZO-II exhibited enhanced capacity (28.72 $mg \cdot g^{-1}$), stability (0.12% Ti^{4+} dissolution), and faster equilibrium (4 h) with Li^+/Na^+ separation factor α = 132.27 [95]. DFT calculations confirmed reduced dehydra-

tion energy barriers, facilitating ion exchange. Dual-surfactant (CTAB/F127) templating produced superhydrophilic $H_4Ti_5O_{12}$ (HTO-IV) with ultrathin nanosheet-assembled microspheres [96]. The material demonstrated exceptional hydrophilicity and hierarchical mesoporous structure, achieving >85% Li^+ removal within 30 min, 57.90 $mg \cdot g^{-1}$ theoretical capacity, and 97% retention after five cycles with Li^+/Na^+ separation factor α = 121.01. Hydroxyethyl cellulose (HEC)-based porous foam (HTO-HEC) utilized -OH group hydrogen bonding to accelerate dehydration kinetics, reducing equilibrium time from 5 h to 1 h [97]. Optimal HTO-HEC-60 achieved 27.9 $mg \cdot g^{-1}$ capacity with Li^+/Na^+ separation factor α = 80.86, maintaining 97.8% capacity after eight cycles with only 0.06% Ti dissolution. Facet-dependent adsorption studies compared flower-shaped (176.23 $m^2 \cdot g^{-1}$) and octahedral (83.02 $m^2 \cdot g^{-1}$) $Li_4Ti_5O_{12}$. Despite lower surface area, octahedral $H_4Ti_5O_{12}$ (111) showed superior capacity (33.56 $mg \cdot g^{-1}$), selectivity (α = 120.10), and cyclic stability (88.9% retention) compared to $H_4Ti_5O_{12}$ (110) (26.85 mg/g, 76.3% retention), attributed to specific facet characteristics including confined pore channels and favorable migration pathways [98].

Despite the unparalleled acid resistance and structural robustness exhibited by titanium-based ion sieves—key advantages over their manganese-based counterparts—their widespread industrial application remains constrained by the inherent trade-off between selectivity and kinetics. Furthermore, synthesis routes that rely on harsh acids and the high cost of titanium precursors pose significant economic barriers. Future research should not only continue to explore atomic-level doping and facet engineering to lower dehydration energy barriers but should also prioritize continuous fixed-bed column tests using real complex brines. Moreover, coupling TIS with membrane technologies or developing binder-free electrode-type adsorbents holds promise for paving the way toward next-generation, energy-efficient lithium recovery systems.

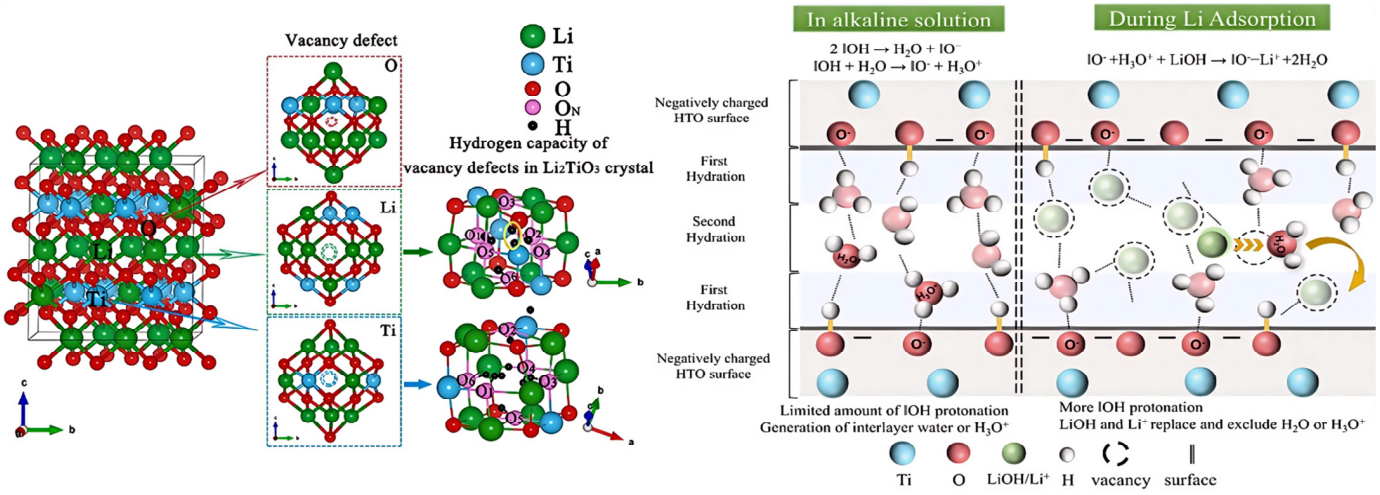


Figure 3. HTO crystal structure and lithium adsorption mechanism of HTO (adapted from [88,89]).

Table 4. Adsorption performance of titanium-based ion sieve adsorption materials.

Adsorbent	Li^+ Concentration ($mg \cdot L^{-1}$)	pH	Adsorption Capacity ($mg \cdot g^{-1}$)	Selectivity α(Li/Na)	Ref.
HTO-$H_2Ti_2O_3$	2000	-	39.2	-	[79]
HTO-$H_2Ti_2O_3$	7000	11.02	94.45	705.3	[80]
HTO-$H_2Ti_2O_3$	669	10	40.16	3414.69	[82]
HTO-$H_2Ti_2O_3$	200	12	34.2	19.96	[83]
HTO-$H_2Ti_2O_3$	1950	13	34.27	350.99	[84]
HTO-$H_2Ti_2O_3$	347	-	39.8	29.46	[90]

Table 4. *Cont.*

Adsorbent	Li^+ Concentration ($mg \cdot L^{-1}$)	pH	Adsorption Capacity ($mg \cdot g^{-1}$)	Selectivity α(Li/Na)	Ref.
HTO-$H_2Ti_2O_3$	2000	12	27.8	37.5	[91]
HTO-$H_2Ti_2O_3$	1950	10.1	16.68	3.44	[92]
HTO-$H_2Ti_2O_3$	82.9	12	32.8	27.11	[93]
HTO-$H_4Ti_5O_{12}$	166.6	14	28.89	-	[94]
HTO-$H_4Ti_5O_{12}$	3470.5	12	15.62	132.27	[95]
HTO-$H_4Ti_5O_{12}$	150	12	30.10	121.01	[96]
HTO-$H_4Ti_5O_{12}$	100	12	30.9	80.86	[97]
HTO-$H_4Ti_5O_{12}$	166.6	13	29.85	120.10	[98]

2.3.2. Manganese-Based Ion Sieve

Manganese-based ion sieves (lithium manganese oxides, LMOs) are recognized as one of the most promising adsorbent materials for lithium extraction from salt lake brines, owing to their high theoretical adsorption capacity, excellent selectivity, and low raw material cost. Depending on the Li/Mn ratio and differences in crystal structure, LMOs can be categorized into three types: $LiMn_2O_4$, $Li_{1.33}Mn_{1.67}O_4$ (i.e., $Li_4Mn_5O_{12}$), and $Li_{1.6}Mn_{1.6}O_4$ (i.e., $Li_2Mn_2O_5$), with theoretical maximum adsorption capacities of 39.9 $mg \cdot g^{-1}$, 59.5 $mg \cdot g^{-1}$, and 72.8 $mg \cdot g^{-1}$, respectively [99–105]. In recent years, extensive research has been conducted on morphology control, doping modifications, and adsorption mechanisms of manganese-based ion sieves, leading to a series of significant advances (Table 5).

In terms of basic material development, studies have demonstrated that porous HMn_2O_4 material exhibits excellent adsorption kinetics, with a saturated lithium adsorption capacity of 30.83 $mg \cdot g^{-1}$ [106]. After ten consecutive adsorption–desorption cycles, the material could still maintain 91.85% of its initial adsorption capacity, indicating good structural stability and cycling regeneration performance [106]. Similarly, a lithium-rich ion sieve (M-LMO-t) synthesized via a microwave-assisted hydrothermal method achieved a lithium adsorption capacity of 38.4 $mg \cdot g^{-1}$ in an alkaline lithium chloride solution (initial concentration 350 $mg \cdot L^{-1}$, pH = 12), which surpassed the performance of the H-LMO material prepared by the conventional hydrothermal method [99]. Regarding crystal structure and synthesis strategies, Zhang et al. [107] reported a simple method for synthesizing a hexagonal spinel-structured $LiMn_2O_4$ (LMO) precursor under mild conditions, and the material was suitable for rapid lithium adsorption–desorption processes. Experimental data show that its acid-modified product (HMO) achieved a lithium adsorption capacity of 24.7 $mg \cdot g^{-1}$, along with a high lithium/sodium selectivity coefficient of 36.7.

To address the intrinsic drawbacks of manganese dissolution and cycling degradation in manganese-based materials, elemental doping and surface modification have become research hotspots. The partition coefficient (Kd) for lithium was significantly higher than that for sodium, demonstrating its excellent ion selectivity. A spinel-type $H_{1.6}Mn_{1.6}O_4$ ion sieve was successfully prepared by Sun et al. [108], with a focus on the regulatory effects of redox precipitation and solid-state reaction on its structure and ion exchange performance. The results indicated that this ion sieve possesses significant selective adsorption capability for lithium from the Qaidam Salt Lake brine (adsorption capacity of 3.88 $mmol \cdot g^{-1}$), providing an important reference for extracting lithium from low-grade salt lake resources. Investigation into the adsorption isotherms, kinetics, and thermodynamics of a surface-fluorinated manganese-based ion sieve adsorption material (F-LMO) revealed that its adsorption behavior conforms to the Langmuir isotherm model and the pseudo-second-order kinetic model [109]. This confirms that the adsorption reaction is a spontaneous chemical adsorption process with uniform adsorption sites. After five adsorption–desorption cycles, F-LMO exhibited a higher adsorption capacity (26.74 $mg \cdot g^{-1}$, capacity retention rate of 91.29%) and a lower manganese dissolution loss rate (1.58%) compared to the pristine LMO.

Wang et al. [110] used LiOH and $MnCO_3$ as raw materials, and a lanthanum (La)-doped $H_{1.6}Mn_{1.6}O_4$ lithium ion sieve (denoted as La-HMO) was prepared. Its adsorption behavior followed the pseudo-second-order kinetic model and the Langmuir isotherm adsorption model. In lithium extraction experiments, La-HMO demonstrated high adsorption capacity and excellent selectivity. After five cycles of use, its adsorption capacity remained at 33.10 mg/g, superior to the 26.80 $mg \cdot g^{-1}$ of the undoped HMO. A spinel-type $H_4Mn_5O_{12}$ ion sieve was prepared by Zhang et al. [111], using a combined method of hydrothermal synthesis and low-temperature solid-state reaction. Experimental results showed that its equilibrium lithium adsorption capacity was significantly enhanced, reaching 6.62 $mmol \cdot g^{-1}$. Even when the initial lithium concentration was as low as 5.0 $mmol \cdot L^{-1}$, the adsorption capacity could still be maintained at approximately 5 $mmol \cdot g^{-1}$.

Luo et al. [112] prepared a manganese-based lithium ion sieve ($H_4Mn_5O_{12}$), indicating that its adsorption of Li^+ is a spontaneous endothermic process conforming to the Langmuir isotherm model and the pseudo-second-order kinetic model. The apparent activation energy for adsorption was 13.52 $kJ \cdot mol^{-1}$, confirming a chemical adsorption mechanism. Furthermore, this ion sieve exhibited significant selectivity for Li^+. After five adsorption–desorption cycles, the adsorption capacity was maintained at 25.46 $mg \cdot g^{-1}$ (82.98% of the initial value), while the manganese dissolution loss rate decreased from 5.49% to 2.77%. A $Li_4Mn_5O_{12}$ precursor with a nanotubular morphology was prepared via a hydrothermal solid-state reaction method, followed by acid washing to obtain $H_4Mn_5O_{12}$ [113]. Adsorption experiments demonstrated a maximum Li^+ adsorption capacity as high as 37.0 $mg \cdot g^{-1}$, and the adsorption process fitted the Langmuir model. Coexisting cation experiments further confirmed that Na^+, K^+, Ca^{2+}, and Mg^{2+} had minimal influence on lithium recovery. Based on the analysis of isothermal adsorption and kinetic characteristics (such as L-type isotherm, pseudo-second-order kinetics model), the adsorption mechanism of $H_4Mn_5O_{12}$ for lithium can be attributed to the electrostatic interaction and ion exchange between Li^+ and H^+.

Manganese-based ion sieves exhibit outstanding adsorption capacity and selectivity (Figure 4). Particularly through nanostructure construction (e.g., nanotubes, porous architectures) and heteroatom doping (e.g., La, F), significant breakthroughs have been achieved in enhancing kinetics, suppressing manganese dissolution, and improving adaptability to low-concentration lithium solutions. However, structural collapse and manganese leaching during long-term cycling remain the core bottlenecks hindering large-scale industrial applications. Future research should further focus on core–shell structure design, the development of novel green eluents, and the validation of continuous fixed-bed adsorption–desorption processes using real complex salt lake brines, thereby facilitating the transition of manganese-based ion sieves from laboratory research to industrial implementation.

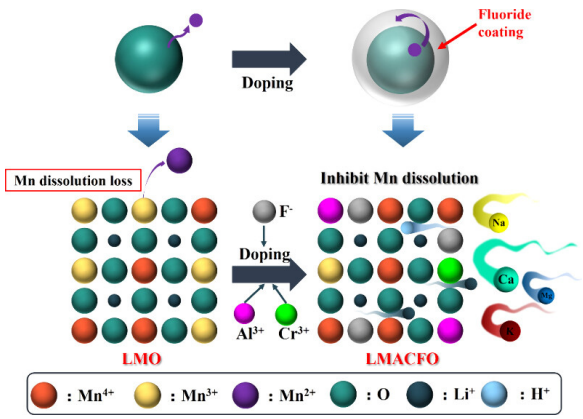


Figure 4. Adsorption mechanism of Mn-based ion sieve (adapted from [114]).

Table 5. Adsorption performance of Mn-based ion sieve adsorption materials.

Adsorbent	Li^+ Concentration ($mg \cdot L^{-1}$)	pH	Adsorption Capacity ($mg \cdot g^{-1}$)	Selectivity α(Li/Na)	Ref.
HMn_2O_4	201	12	38.4	938.4	[99]
$H_{1.6}Mn_{1.6}O_4$	100	12	33.10	21.65	[110]
$H_4Mn_5O_{12}$	1000	12.5	31.48	12.22	[112]
$H_4Mn_5O_{12}$	185.8	12	37.0	-	[113]

3. Conclusions

This review has comprehensively examined the state-of-the-art adsorption technologies for recovering lithium from challenging low-grade resources, particularly high-Na/Li-ratio brines like lithium precipitation mother liquor. A comparative analysis reveals that each class of adsorbent possesses distinct advantages and limitations, governed by its unique separation mechanism.

Organic adsorbents, particularly crown ether-based materials, achieve exceptional Li^+/Na^+ selectivity (α up to thousands) via precise cavity size matching, but their practical application is often constrained by synthesis cost, solvent use, and the need for robust support materials.

Inorganic adsorbents present a more diverse and scalable portfolio. Aluminum-based LDHs benefit from established synthesis methods and good stability, though their adsorption capacity is generally modest. Titanium-based ion sieves (e.g., H_2TiO_3, $H_4Ti_5O_{12}$) stand out for their high theoretical capacity, remarkable acid stability, and excellent cycling performance; however, slow adsorption kinetics remains a key challenge. Manganese-based ion sieves (e.g., HMn_2O_4, $H_4Mn_5O_{12}$) often exhibit superior ion exchange technique and high capacity, but their commercial viability is hampered by manganese dissolution during cycling, which compromises structural integrity and causes secondary pollution.

The path forward for the industrial implementation of adsorption-based lithium recovery lies in targeted material and process engineering. Future research should prioritize the following: (1) Performance Enhancement: Designing adsorbents with optimized morphology (e.g., nanosheets, nanotubes), controlled particle size, tailored porosity, and doped/co-doped structures to simultaneously improve capacity, selectivity, and kinetics while inhibiting ion dissolution. (2) Process Scalability and Economics: Developing cost-effective, environmentally benign synthesis routes and efficient regeneration protocols to reduce operational costs. (3) System Integration: Exploring hybrid processes that intelligently combine adsorption with other unit operations (e.g., membrane filtration, precipitation) to overcome the limitations of any single technology, thereby improving overall recovery efficiency, product purity, and process sustainability. Addressing these challenges will be crucial for securing a stable and sustainable lithium supply chain to support the global clean energy transition.

Author Contributions: Conceptualization, X.M., H.Z., X.Z., and C.Z.; validation, X.M., H.Z., and X.Z.; formal analysis, X.M., H.Z., Y.J., Y.S., and S.Z.; investigation, S.Z., Y.S., and C.Z.; resources, Y.J.; writing—original draft preparation, X.M. and H.Z.; writing—review and editing, X.M. and H.Z.; visualization, X.M. and H.Z.; supervision, H.Z.; project administration, X.Z.; funding acquisition, Y.J. All authors have read and agreed to the published version of the manuscript.

Funding: This research was funded by the National Key Research and Development Program, grant number 2021YFC2903. The APC was funded by the Technical Center for Pyrometallurgy, BGRIMM Engineering Technology Co., Ltd., BGRIMM Technology Group, Beijing 100160, China.

Data Availability Statement: No new data were created or analyzed in this study.

Conflicts of Interest: All authors were employed by the Technical Center for Pyrometallurgy, BGRIMM Engineering Technology Co., Ltd., BGRIMM Technology Group, Beijing 100160, China. The authors declare that the APC for this article was funded by the Technical Center for Pyrometallurgy, BGRIMM Engineering Technology Co., Ltd., BGRIMM Technology Group, Beijing 100160, China. The company was not involved in the study design, collection, analysis, interpretation of data, the writing of this article or the decision to submit it for publication.

References

1. Halder, P.; Joardder, N.; Sarker, M. Energy scarcity and potential of renewable energy in Bangladesh. *Renew. Sustain. Energy Rev.* **2015**, *51*, 1636–1649. [CrossRef]
2. Ellabban, O.; Blaabjerg, F. Renewable energy resources: Current status, future prospects and their enabling technology. *Renew. Sustain. Energy Rev.* **2014**, *39*, 748–764. [CrossRef]
3. He, S.; Zuo, Q.; Shi, H.; Geng, Z.; Liu, C.; Ding, L.; Li, X.; Shao, P.; Yang, L.; Luo, X. Direct recovery of high-purity lithium via nanofiltration membranes from leaching solution of spent lithium batteries. *Resour. Conserv. Recycl.* **2024**, *210*, 107846. [CrossRef]
4. Choi, J.; Aurbach, D. Promise and reality of post-lithium-ion batteries with high energy densities. *Nat. Rev. Mater.* **2016**, *1*, 16013. [CrossRef]
5. Li, Z.; Wang, C.; Chen, J. Supply and demand of lithium in China based on dynamic material flow analysis. *Renew. Sustain. Energy Rev.* **2024**, *203*, 114786. [CrossRef]
6. U.S. Geological Survey. *Mineral Commodity Summaries 2023*; U.S. Geological Survey: Reston, VA, USA, 2023.
7. Chen, W.; Li, X.; Chen, L.; Zhou, G.; Lu, Q.; Huang, Y.; Chao, Y.; Zhu, W. Tailoring hydrophobic deep eutectic solvent for selective lithium recovery from the mother liquor of Li_2CO_3. *Chem. Eng. J.* **2021**, *420*, 127648. [CrossRef]
8. Kanagasundaram, T.; Murphy, O.; Haji, M.N.; Wilson, J.J. The recovery and separation of lithium by using solvent extraction methods. *Coord. Chem. Rev.* **2024**, *509*, 215727. [CrossRef]
9. Danso, D.K.; Alhajeri, M.M.; Bicerano, J.; Heller, D.P.; Longe, P.O.; Ghahfarokhi, R.B. A review of polyelectrolytes and their complexes for lithium recovery from oilfield and geothermal brines. *Appl. Energy* **2025**, *392*, 125966. [CrossRef]
10. Knapik, E.; Rotko, G.; Marszałek, M. Recovery of lithium from oilfield brines—Current achievements and future perspectives: A mini review. *Energies* **2023**, *16*, 6628. [CrossRef]
11. Vera, M.; Torres, W.; Galli, C.; Chagnes, A.; Flexer, V. Environmental impact of direct lithium extraction from brines. *Nat. Rev. Earth Environ.* **2023**, *4*, 149–165. [CrossRef]
12. Meshram, P.; Pandey, B.; Mankhand, T. Extraction of lithium from primary and secondary sources by pre-treatment, leaching and separation: A comprehensive review. *Hydrometallurgy* **2014**, *150*, 192–208. [CrossRef]
13. Abe, Y. Rare Metal Series—Current Status of Lithium Resources. In *JOGMEC Mineral Resources Report*; Japan Oil, Gas and Metals National Corporation (JOGMEC): Chiba, Japan, 2010.
14. Yang, Y.; Wang, F.; Pan, X.; Yang, T.; Hu, S.; Tang, S.; Jia, Q. Solid membrane-based aqueous lithium extraction and adsorption: Advances, challenges, and prospects. *Chem. Eng. J.* **2025**, *510*, 161748. [CrossRef]
15. Li, Y.; Dong, L.; Shi, P.; Li, Y.; Yang, H.; Zheng, N.; Ren, Z.; Zhou, Z. Selective leaching and recovery of lithium ions from lithium slag with low lithium content. *Can. J. Chem. Eng.* **2025**, *103*, 5635–5647. [CrossRef]
16. Zhang, L.; Li, L.; Shi, D.; Li, J.; Peng, X.; Nie, F. Selective extraction of lithium from alkaline brine using HBTA-TOPO synergistic extraction system. *Sep. Purif. Technol.* **2017**, *188*, 167–173. [CrossRef]
17. Xing, M.; Zhang, F.; Zheng, P.; Wang, Y.; Zhao, L.; Xu, C. Selective recovery of lithium from high-aluminum fly ash by using alkali-dissolution-assisted HBTA-TOPO synergistic extraction. *J. Clean. Prod.* **2024**, *434*, 139998. [CrossRef]
18. Ma, Y.; Huang, S.; Liu, X.; Huang, J.; Zhang, Y.; Li, K.; Zhang, Z.; Yu, X.; Fu, Z. Lithium enrichment and migration mechanism in the evaporation process of sodium sulphate subtype salt lake brine. *Desalination* **2023**, *566*, 116908. [CrossRef]
19. Li, X.; Mo, Y.; Qing, W.; Shao, S.; Tang, C.; Li, J. Membrane-based technologies for lithium recovery from water lithium resources: A review. *J. Membr. Sci.* **2019**, *591*, 117317. [CrossRef]
20. Coterillo, R.; Gallart, L.; Fernandez-Escalante, E.; Junquera, J.; Garcia-Fernandez, P.; Ortiz, I.; Ibanez, R.; San-Roman, M. Selective extraction of lithium from seawater desalination concentrates: Study of thermodynamic and equilibrium properties using Density Functional Theory (DFT). *Desalination* **2022**, *532*, 115704. [CrossRef]
21. Hu, H.; Guo, X.; Yang, L.; Wu, Y.; Yang, G.; Luo, X. Adsorption materials toward highly-efficient lithium extraction from Non-Conventional lithium sources. *Adv. Mater.* **2025**, *37*, e2506055. [CrossRef] [PubMed]
22. Zhang, J.; Chen, T.; Ma, L.; Hai, C.; Sun, Y.; Dong, S.; He, X.; Xu, Q.; Chen, J.; Su, H.; et al. Factors affecting the efficiency of electrochemical lithium extraction: A systematic review from materials to processes technology. *Desalination* **2025**, *602*, 118570. [CrossRef]

23. Ighalo, J.; Amaku, J.; Olisah, C.; Adeola, A.; Iwuozor, K.; Akpomie, K.; Conradie, J.; Adegoke, K.; Oyedotun, K. Utilisation of adsorption as a resource recovery technique for lithium in geothermal water. *J. Mol. Liq.* **2022**, *365*, 120107. [CrossRef]
24. Lu, B.; Lin, W.; Yang, H.; Pei, J.; Ye, P.; Liu, Y.; Jiang, F.; Lu, Z.; Xu, Z. Recent advances in design of titanium-based lithium ion-sieves for lithium extraction from salt lakes: Synthesis, crystal structures and adsorption mechanisms. *Chem. Eng. J.* **2025**, *525*, 169829. [CrossRef]
25. Liu, G.; Zhao, Z.; Ghahreman, A. Novel approaches for lithium extraction from salt-lake brines: A review. *Hydrometallurgy* **2019**, *187*, 81–100. [CrossRef]
26. Evans, B.; Jayanthi, K.; Popovs, I.; Moyer, B.; Paranthaman, M. New directions and principles for solvent extraction for recovery of lithium from aqueous brines and mineral leachates: A brief review. *Sustain. Mater. Technol.* **2025**, *46*, e01724. [CrossRef]
27. Adeyanju, C.; Ogunniyi, S.; Selvasembian, R.; Oniye, M.; Ajala, O.; Adeniyi, A.; Igwegbe, C.; Ighalo, J. Recent advances on the aqueousphaseadsorption of carbamazepine. *ChemBioEng Rev.* **2022**, *9*, 231–247. [CrossRef]
28. Ogunlalu, I.; Iwuozor, K.; Aderibigbe, A.; Emenike, E. Trends in the mitigation of heavy metal ions from aqueous solutions using unmodified and chemically-modified agricultural waste adsorbents. *Curr. Res. Green Sustain. Chem.* **2021**, *4*, 18. [CrossRef]
29. Ighalo, J.; Kurniawan, S.; Iwuozor, K.; Aniagor, C.; Ajala, O.; Oba, S.; Iwuchukwu, F.; Ahmadi, S.; Igwegbe, C. A review of treatment technologies for the mitigation of the toxic environmental effects of acid mine drainage (AMD). *Process Saf. Environ. Prot.* **2022**, *157*, 37–58. [CrossRef]
30. Iwuozor, K.; Abdullahi, T.; Ogunfowora, L.; Emenike, E.; Oyekunle, I.; Gbadamosi, F.; Ighalo, J. Mitigation of levofloxacin from aqueous media by adsorption: A review. *Sustain. Water Resour. Manag.* **2021**, *7*, 100. [CrossRef]
31. Xu, J.; Wei, X.; Han, J.; Qin, W. Synthesis and optimisation mechanism of functionalised adsorption materials for lithium-ion extraction from salt water: A review. *Sep. Purif. Technol.* **2024**, *339*, 126237. [CrossRef]
32. Onishi, K.; Nakamura, T.; Nishihama, S.; Yoshizuka, K. Synergistic solvent impregnated resin for adsorptive separation of lithium ion. *Ind. Eng. Chem. Res.* **2010**, *49*, 6554–6558. [CrossRef]
33. Wu, Y.; Guo, W.; Sun, Y.; Sun, S. Resin functionalized with 2-(hydroxymethyl)-12-crown-4 ether for selective adsorption of lithium ions from desilication solution of coal-based solid waste. *Sep. Purif. Technol.* **2025**, *355*, 129500. [CrossRef]
34. Liu, X.; Zhong, M.; Chen, X.; Zhao, Z. Separating lithium and magnesium in brine by aluminum-based materials. *Hydrometallurgy* **2018**, *176*, 73–77. [CrossRef]
35. Zandevakili, S.; Ranjbar, M.; Ehteshamzadeh, M. Improvement of lithium adsorption capacity by optimising the parameters affecting synthesised ion sieves. *Micro Nano Lett.* **2015**, *10*, 58–63. [CrossRef]
36. Torrejos, R.; Nisola, G.; Park, M.; Shon, H.; Seo, J.; Koo, S.; Chung, W. Synthesis and characterization of multi-walled carbon nanotubes-supported dibenzo-14-crown-4 ether with proton ionizable carboxyl sidearm as Li^+ adsorbents. *Chem. Eng. J.* **2015**, *264*, 89–98. [CrossRef]
37. Hangarge, R.; La, D.; Boguslavsky, M.; Jones, L.; Kim, Y.; Bhosale, S. An Aza-12-crown-4 Ether-substituted naphthalene diimide chemosensor for the detection of lithium ion. *ChemistrySelect* **2017**, *2*, 11487–11491. [CrossRef]
38. Pedersen, C. Cyclic polyethers and their complexes with metal salts. *J. Am. Chem. Soc.* **1967**, *89*, 7017–7036. [CrossRef]
39. Torrejos, R.; Nisola, G.; Song, H.; Limjuco, L.; Lawagon, C.; Parohinog, K.; Koo, S.; Han, J.; Chung, W. Design of lithium selective crown ethers: Synthesis, extraction and theoretical binding studies. *Chem. Eng. J.* **2017**, *326*, 921–933. [CrossRef]
40. Nisola, G.; Parohinog, K.; Cho, M.; Burnea, F.; Lee, J.; Seo, J.; Lee, S.; Chung, W. Covalently decorated crown ethers on magnetic graphene oxides as bi-functional adsorbents with tailorable ion recognition properties for selective metal ion capture in water. *Chem. Eng. J.* **2020**, *389*, 123421. [CrossRef]
41. Awual, M. Ring size dependent crown ether based mesoporous adsorbent for high cesium adsorption from wastewater. *Chem. Eng. J.* **2016**, *303*, 539–546. [CrossRef]
42. Wang, P.; Dai, J.; Ma, Y.; Chen, L.; Pan, J. Fabrication and evaluation of aminoethyl benzo-12-crown-4 functionalized polymer brushes adsorbents formed by surface-initiated ATRP based on macroporous polyHIPEs and postsynthetic modification. *Chem. Eng. J.* **2020**, *380*, 122495. [CrossRef]
43. Xu, X.; Qiu, F.; Yang, D.; Zheng, X.; Wang, Y.; Pan, J.; Zhang, T.; Xu, J.; Li, C. Dual-template crown ether-functionalized hierarchical porous silica: Preparation and application for adsorption of energy metal lithium. *Appl. Organomet. Chem.* **2018**, *32*, 4114. [CrossRef]
44. Hankins, M.; Hayashita, T.; Kasprzyk, S.; Bartsch, R. Immobilization of crown ether carboxylic acids on silica gel and their use in column concentration of alkali metal cations from dilute aqueous solutions. *Anal. Chem.* **1996**, *68*, 2811–2817. [CrossRef] [PubMed]
45. Awual, M.R.; Suzuki, S.; Taguchi, T.; Shiwaku, H.; Okamoto, Y.; Yaita, T. Radioactive cesium removal from nuclear wastewater by novel inorganic and conjugate adsorbents. *Chem. Eng. J.* **2014**, *242*, 127–135. [CrossRef]
46. Qin, W.; Xu, S.; Xu, G.; Xie, Q.; Wang, C.; Xu, Z. Preparation of silica gel bound crown ether and its extraction performance towards zirconium and hafnium. *Chem. Eng. J.* **2013**, *225*, 528–534. [CrossRef]

47. FavreReguillon, A.; Dumont, N.; Dunjic, B.; Lemaire, M. Polymeric and immobilized crown compounds, material for ion separation. *Tetrahedron* **1997**, *53*, 1343–1360. [CrossRef]
48. Alexandratos, S.; Stine, C.; Sachleben, R.; Moyer, B. Immobilization of lithium-selective 14-crown-4 on crosslinked polymer supports. *Polymer* **2005**, *46*, 6347–6352. [CrossRef]
49. Hayashita, T.; Lee, J.; Hankins, M.; Lee, J.; Kim, J.; Knobeloch, J.; Bartsch, R. Selective sorption and column concentration of alkali-metal cations by carboxylic-acid resins with dibenzo-14-crown-4 subunits and their acyclic polyether analogs. *Anal. Chem.* **1992**, *64*, 815–819. [CrossRef]
50. Yang, F.; Hua, J.; Du, J.; He, J.; Xiao, J.; Li, L.; Ma, X.; Li, J. Electrospun nanofiber membrane of 14-crown-4 polyimide by in situ grafting diamino crown ether for highly selective Li plus adsorption and separation. *Sep. Purif. Technol.* **2024**, *351*, 128097. [CrossRef]
51. Huang, Y.; Li, X.; Chen, L.; Luo, G.; Tao, D.; Sun, J.; Qiu, Z.; Chao, Y.; Zhu, W. Synthesis of a magnetic crown ether ion imprinted polymer material for the selective adsorption of lithium. *New J. Chem.* **2023**, *47*, 3134–3139. [CrossRef]
52. Zhu, Q.; Ma, X.; Pei, H.; Li, J.; Yan, F.; Cui, Z.; Wang, H.; Li, J. A highly-efficient lithium adsorptive separation membrane derived from a polyimide-containing dibenzo-14-crown-4 moiety. *Sep. Purif. Technol.* **2020**, *247*, 116940. [CrossRef]
53. Ali, M.; Ahmed, I.; Ramirez, P.; Nasir, S.; Mafe, S.; Niemeyer, C.M.; Ensinger, W. Lithium ion recognition with nanofluidicdiodes through host-guest complexation in confined geometries. *Anal. Chem.* **2018**, *90*, 6820–6826. [CrossRef] [PubMed]
54. Luo, X.; Guo, B.; Luo, J.; Deng, F.; Zhang, S.; Luo, S.; Crittenden, J. Recovery of lithium from wastewater using development of Li ion-imprinted polymers. *ACS Sustain. Chem. Eng.* **2015**, *3*, 460–467. [CrossRef]
55. Inokuchi, Y.; Ebata, T.; Rizzo, T. Microhydration of Dibenzo-18-Crown-6 complexes with K^+, RID^+, and Cs^+ investigated by cold UV and IR spectroscopy in the gas phase. *J. Phys. Chem. A* **2018**, *122*, 3754–3763. [CrossRef] [PubMed]
56. Mou, B. Preparation and Performance Study of Lithium Adsorbents Based on LiAl-LDH Composites. Master's Thesis, University of Chinese Academy of Sciences, Qinghai, China, 2025.
57. Chen, L. Study on Lithium Extraction from Salt Lake Brine by Adsorption. Master's Thesis, Beijing University of Chemical Technology, Beijing, China, 2020.
58. Feng, L. Preparation of Modified Aluminum Adsorbent and Study on Lithium Extraction Performance. Master's Thesis, Liaoning University, Shenyang, China, 2023.
59. Zhang, L.; Zhang, T.; Zhao, Y.; Dong, G.; Lv, S.; Ma, S.; Song, S.; Quintana, M. Doping engineering of lithium-aluminum layered double hydroxides for high-efficiency lithium extraction from salt lake brines. *Nano Res.* **2024**, *17*, 1646–1654. [CrossRef]
60. Ping Liu, C.; Guo, J.; Yu, F.; Ma, X. Synthesis of lithium aluminum layered double hydroxide/kaolinite composite adsorbents and application for lithium extraction from brines. *Ind. Eng. Chem. Res.* **2026**, *65*, 13349–13358. [CrossRef]
61. Pan, Y.; Zhang, W. Impurity Shielding in Li/Al-LDH-based lithium recovery from produced water via activated carbon pretreatment. *ACS Sustain. Chem. Eng.* **2025**, *13*, 14527–14539. [CrossRef] [PubMed]
62. Wu, Z.; Xie, Z.; Wang, J.; Yu, T.; Wang, Z.; Hao, X.; Abudula, A.; Guan, G. Lithium-salt-containing ionic liquid-incorporated Li-Al-Layered double hydroxide-based solid electrolyte with high-performance and safety in solid-state lithium batteries. *ACS Sustain. Chem. Eng.* **2020**, *8*, 12378–12387. [CrossRef]
63. Luo, Q.; Dong, M.; Nie, G.; Liu, Z.; Wu, Z.; Li, J. Extraction of lithium from salt lake brines by granulated adsorbents. *Colloids Surf. A-Physicochem. Eng. Asp.* **2021**, *628*, 127256. [CrossRef]
64. Zhang, F.; Hou, W. Mechano-hydrothermal preparation of Li-Al-OH layered double hydroxides. *Solid State Sci.* **2018**, *79*, 93–98. [CrossRef]
65. Qin, Y.; Yang, T.; Shi, C.; Liu, B. Adsorption of lithium ions from aqueous solution by magnetic aluminum-based adsorbents. *PLoS ONE* **2023**, *18*, e0295269. [CrossRef] [PubMed]
66. Zhong, J.; Lin, S.; Yu, J. Li^+ adsorption performance and mechanism using lithium/aluminum layered double hydroxides in low grade brines. *Desalination* **2021**, *505*, 114983. [CrossRef]
67. Wu, J.; Liu, B.; Qian, J.; Tao, Y.; Lin, C.; Wang, R.; Gao, J.; Xia, Y. Facile synthesis of aluminum-based adsorbents from spent lithium-ion batteries for efficient Li^+ extraction. *J. Environ. Chem. Eng.* **2025**, *13*, 117000. [CrossRef]
68. Luo, Q.; Dong, M.; Li, Q.; Wu, Z.; Liu, Z.; Li, J. Improve the durability of lithium adsorbent Li/Al-LDHs by Fe^{3+} substitution and nanocomposite of FeOOH. *Miner. Eng.* **2022**, *185*, 107717. [CrossRef]
69. Huo, J.; Hai, C.; Li, Y.; Sun, Y.; Dong, S.; Ma, L.; He, X.; Xu, Q.; Zhou, Y. Configuring a structure self-curable lithium aluminum layered double hydroxide chloride type lithium adsorbents via a facile one-pot synergistical modification way. *Chem. Eng. J.* **2024**, *498*, 155258. [CrossRef]
70. Zhang, L.; Li, Y.; Qiao, X.; Li, R.; Li, T.; Cheng, P.; Zhang, J.; Tang, N. Carbonate-intercalated aluminum layered double hydroxide for high-capacity lithium extraction. *Desalination* **2025**, *615*, 119307. [CrossRef]
71. Orooji, Y.; Nezafat, Z.; Nasrollahzadeh, M.; Shafiei, N.; Afsari, M.; Pakzad, K.; Razmjou, A. Recent advances in nanomaterial development for lithium ion-sieving technologies. *Desalination* **2022**, *529*, 115624. [CrossRef]

72. Chitrakar, R.; Makita, Y.; Ooi, K.; Sonoda, A. Lithium recovery from salt lake brine by H_2TiO_3. *Dalton Trans.* **2014**, *43*, 8933–8939. [CrossRef] [PubMed]
73. Denisova, T.; Maksimova, L.; Polyakov, E.; Zhuravlev, N.; Kovyazina, S.; Leonidova, O.; Khabibulin, D.; Yur'eva, E. Metatitanic acid: Synthesis and properties. *Russ. J. Inorg. Chem.* **2006**, *51*, 691–699. [CrossRef]
74. Wang, S.; Li, P.; Cui, W.; Zhang, H.; Wang, H.; Zheng, S.; Zhang, Y. Hydrothermal synthesis of lithium-enriched β-Li2TiO3 with an ion-sieve application: Excellent lithium adsorption. *RSC Adv.* **2016**, *6*, 102608–102616. [CrossRef]
75. Weng, D.; Duan, H.; Hou, Y.; Huo, J.; Chen, L.; Zhang, F.; Wang, J. Introduction of manganese based lithium-ion Sieve-A review. *Prog. Nat. Sci. Mater. Int.* **2020**, *30*, 139–152. [CrossRef]
76. Wang, S.; Li, P.; Zhang, X.; Zheng, S.; Zhang, Y. Selective adsorption of lithium from high Mg-containing brines using HxTiO3 ion sieve. *Hydrometallurgy* **2017**, *174*, 21–28. [CrossRef]
77. Shi, X.; Zhang, Z.; Zhou, D.; Zhang, L.; Chen, B.; Yu, L. Synthesis of Li^+ adsorbent (H_2TiO_3) and its adsorption properties. *Trans. Nonferrous Met. Soc. China* **2013**, *23*, 253–259. [CrossRef]
78. Zhang, L.; Zhou, D.; Yao, Q.; Zhou, J. Preparation of H_2TiO_3-lithium adsorbent by the sol-gel process and its adsorption performance. *Appl. Surf. Sci.* **2016**, *368*, 82–87. [CrossRef]
79. Zhang, L.; Zhou, D.; He, G.; Wang, F.; Zhou, J. Effect of crystal phases of titanium dioxide on adsorption performance of H_2TiO_3-lithium adsorbent. *Mater. Lett.* **2014**, *135*, 206–209. [CrossRef]
80. Lawagon, C.; Nisola, G.; Mun, J.; Tron, A.; Torrejos, R.; Seo, J.; Kim, H.; Chung, W. Adsorptive Li^+ mining from liquid resources by H_2TiO_3: Equilibrium, kinetics, thermodynamics, and mechanisms. *J. Ind. Eng. Chem.* **2016**, *35*, 347–356. [CrossRef]
81. He, G.; Zhang, L.; Zhou, D.; Zou, Y.; Wang, F. The optimal condition for H_2TiO_3 -lithium adsorbent preparation and Li^+ adsorption confirmed by an orthogonal test design. *Ionics* **2015**, *21*, 2219–2226. [CrossRef]
82. Gu, D.; Sun, W.; Han, G.; Cui, Q.; Wang, H. Lithium ion sieve synthesized via an improved solid state method and adsorption performance for West Taijinar Salt Lake brine. *Chem. Eng. J.* **2018**, *350*, 474–483. [CrossRef]
83. Li, X.; Chao, Y.; Chen, L.; Chen, W.; Luo, J.; Wang, C.; Wu, P.; Li, H.; Zhu, W. Taming wettability of lithium ion sieve via different TiO2 precursors for effective Li recovery from aqueous lithium resources. *Chem. Eng. J.* **2020**, *392*, 123731. [CrossRef]
84. Wang, Q.; Yang, X.; Li, C.; Zhao, C.; Huang, Y.; Qiu, S.; Qin, Y.; Shi, C. Titanium-based lithium ion sieve adsorbent H_2TiO_3 with enhanced Li plus adsorption properties by magnetic Fe doping. *Sep. Purif. Technol.* **2024**, *346*, 127455. [CrossRef]
85. Moazeni, M.; Hajipour, H.; Askari, M.; Nusheh, M. Hydrothermal synthesis and characterization of titanium dioxide nanotubes as novel lithium adsorbents. *Mater. Res. Bull.* **2015**, *61*, 70–75. [CrossRef]
86. Wei, S.; Wei, Y.; Chen, T.; Liu, C.; Tang, Y. Porous lithium ion sieves nanofibers: General synthesis strategy and highly selective recovery of lithium from brine water. *Chem. Eng. J.* **2020**, *379*, 122407. [CrossRef]
87. Nugroho, A.; Kim, S.; Chang, W.; Chung, K.; Kim, J. Facile synthesis of hierarchical mesoporous Li4Ti5O12 microspheres in supercritical methanol. *J. Power Sources* **2013**, *244*, 164–169. [CrossRef]
88. Su, J.; Li, Y.; Wang, W.; Li, K.; Yang, W. Trapping hydrogen atoms in vacancies of Li2TiO3 Crystal: A first-principles study. *ACS Omega* **2022**, *7*, 27149–27156. [CrossRef] [PubMed]
89. Lu, B.; Wang, X.; Zhang, Y.; Wang, Q.; Jiang, F.; Lin, W.; Liu, L.; Ye, P.; Lu, W.; Lu, Z.; et al. Beyond ion exchange: Unraveling the complexity of lithium-ion adsorption on H_2TiO_3. *ACS Appl. Mater. Interfaces* **2025**, *17*, 39628–39641. [CrossRef] [PubMed]
90. Zhiyong, J.; Junsheng, Y.; Xingang, L. Synthesis of Li-adsorbent and its adsorption property. *Chem. Eng.* **2007**, *35*, 9–13.
91. Tang, D.; Zhou, D.; Zhou, J.; Zhang, P.; Zhang, L.; Xia, Y. Preparation of H_2TiO_3-lithium adsorbent using low-grade titanium slag. *Hydrometallurgy* **2015**, *157*, 90–96. [CrossRef]
92. Ji, Z.; Yang, F.; Zhao, Y.; Liu, J.; Wang, N.; Yuan, J. Preparation of titanium-base lithium ionic sieve with sodium persulfate as eluent and its performance. *Chem. Eng. J.* **2017**, *328*, 768–775. [CrossRef]
93. You, R.; He, Z.; Xue, F.; Ju, S. Construction of robust H_2TiO_3@PAM hydrogel ion-sieve via in-situ polymerization for Li^+ adsorption. *Surf. Interfaces* **2025**, *56*, 105697. [CrossRef]
94. Zhao, B.; Qian, Z.; Qiao, Y.; Li, J.; Wu, Z.; Liu, Z. The Li(H_2O)n dehydration behavior influences the Li^+ ion adsorption on $H_4Ti_5O_{12}$ with different facets exposed. *Chem. Eng. J.* **2023**, *451*, 138870. [CrossRef]
95. Xiao, X.; Li, J.; Qiu, K.; Chen, M.; Xie, H. Synergistic effect of Fe/Zr dual doping endows hydrophilic spinel-structured $H_4Ti_5O_{12}$ ion sieves for efficient lithium extraction from liquid resources. *Sep. Purif. Technol.* **2025**, *358*, 130358. [CrossRef]
96. Xiao, X.; Li, J.; Qiu, K.; Chen, M.; Zhang, X. Dual surfactants-assisted adsorption of lithium ions in liquid lithium resources on a superhydrophilic spinel-type $H_4Ti_5O_{12}$ ion sieve. *Sep. Purif. Technol.* **2024**, *330*, 125479. [CrossRef]
97. Yang, C.; Zhang, S.; Lu, H.; Tang, K.; Yang, J.; Shi, L.; Xiong, S.; Tang, A.; Jiang, J. Preparation of $H_4Ti_5O_{12}$-hydroxyethyl cellulose composite for rapid adsorption of lithium in aqueous solution. *Sep. Purif. Technol.* **2025**, *362*, 131852. [CrossRef]
98. Zhao, B.; Qian, Z.; Guo, M.; Wu, Z.; Liu, Z. The performance and mechanism of recovering lithium on $H_4Ti_5O_{12}$ adsorbents influenced by (110) and (111) facets exposed. *Chem. Eng. J.* **2021**, *414*, 128729. [CrossRef]
99. Deng, G.; Jiang, R.; Guan, J.; Tang, F.; Hou, Z.; Feng, Y. Microwave-Synthesized Mn-based Li-rich ion sieves for selective lithium recovery from high Mg/Li brines. *ACS Appl. Energy Mater.* **2025**, *8*, 7273–7282. [CrossRef]

100. Chen, M.; Wu, R.; Ju, S.; Zhang, X.; Xue, F.; Xing, W. Improved performance of Al-doped $LiMn_2O_4$ ion-sieves for Li^+ adsorption. *Microporous Mesoporous Mater.* **2018**, *261*, 29–34. [CrossRef]
101. Zhang, Q.; Li, S.; Sun, S.; Yin, X.; Yu, J. LiMn2O4 spinel direct synthesis and lithium ion selective adsorption. *Chem. Eng. Sci.* **2010**, *65*, 169–173. [CrossRef]
102. Hong, H.; Park, I.; Ryu, T.; Ryu, J.; Kim, B.; Chung, K. Granulation of $Li_{1.33}Mn_{1.67}O_4$ (LMO) through the use of cross-linked chitosan for the effective recovery of Li^+ from seawater. *Chem. Eng. J.* **2013**, *234*, 16–22. [CrossRef]
103. Yang, X.; Kanoh, H.; Tang, W.; Ooi, K. Synthesis of $Li_{1.33}Mn_{1.67}O_4$ spinels with different morphologies and their ion adsorptivities after delithiation. *J. Mater. Chem.* **2000**, *10*, 1903–1909. [CrossRef]
104. Liu, L.; Zhang, H.; Zhang, Y.; Cao, D.; Zhao, X. Lithium extraction from seawater by manganese oxide ion sieve $MnO_2{\cdot}0.5H_2O$. *Colloids Surf. A-Physicochem. Eng. Asp.* **2015**, *468*, 280–284. [CrossRef]
105. Ding, K.; Zhu, G.; Song, C.; Wang, Q.; Wang, L.; Wang, Z.; Meng, C.; Gao, C. Fabrication of polyacrylonitrile-$Li_{1.6}Mn_{1.6}O_4$ composite nanofiber flat-sheet membranes via electrospinning method as effective adsorbents for Li^+ recovery from salt-lake brine. *Sep. Purif. Technol.* **2022**, *284*, 120242. [CrossRef]
106. Dai, Y.; Zhang, X.; Sun, J.; Wu, S.; Zhao, Z.; Xu, W.; Ren, G.; Li, Y.; Liu, D. Porous manganese-based ion sieve for sustainable lithium extraction from brine: High-efficiency adsorption and rapid kinetics. *Desalination* **2025**, *614*, 119168. [CrossRef]
107. Zhang, Q.; Sun, S.; Li, S.; Yin, X.; Yu, J. Direct Hydrothermal Synthesis of Ternary Li-Mn-O Oxide Ion-Sieves. In *Interdisciplinary Transport Phenomena: Fluid, Thermal, Biological, Materials, and Space Sciences*; Sadhal, S.S., Ed.; The New York Academy of Sciences: New York, NY, USA, 2009; Volume 1161, pp. 500–507.
108. Sun, S.; Xiao, J.; Wang, J.; Song, X.; Yu, J. Synthesis and Adsorption Properties of $Li_{1.6}Mn_{1.6}O_4$ by acombination of redoxprecipitation and solid-phase reaction. *Ind. Eng. Chem. Res.* **2014**, *53*, 15517–15521. [CrossRef]
109. Zhang, G.; Zhang, J.; Zeng, J.; Sun, Y.; Shen, Y.; Li, X.; Ren, X.; Hai, C.; Zhou, Y.; Tang, W. Improved structural stability and adsorption capacity of adsorbent material $Li_{1.6}Mn_{1.6}O_4$ via facile surface fluorination. *Colloids Surf. A-Physicochem. Eng. Asp.* **2021**, *629*, 127465. [CrossRef]
110. Wang, Y.; Shi, D.; Cao, Y.; Han, X.; Zhang, T.; Zhong, K.; Zhao, Q.; Xu, N.; Bian, S. La^{3+}doped $H_{1.6}Mn_{1.6}O_4$ lithium-ion sieve for Li plus efficient adsorption and analysing anti-dissolution loss mechanism. *Particuology* **2025**, *106*, 201–212. [CrossRef]
111. Zhang, Q.; Li, S.; Sun, S.; Yin, X.; Yu, J. Lithium selective adsorption on 1-D MnO_2 nanostructure ion-sieve. *Adv. Powder Technol.* **2009**, *20*, 432–437. [CrossRef]
112. Luo, J.; Shu, J.; Zhao, H.; Wang, J.; Chen, S.; Yang, H.; Lin, F.; Zhang, S.; Chen, M.; Yang, Y. Synthesis of lithium-ion sieves based on electrolytic manganese anode slime: Characterization and its lithium adsorption performance. *Chem. Eng. J.* **2025**, *523*, 168001. [CrossRef]
113. Xu, N.; Li, S.; Guo, M.; Qian, Z.; Li, W.; Liu, Z. Synthesis of $H_4Mn_5O_{12}$ nanotubes lithium ion sieve and its adsorption properties for Li^+ from aqueous solution. *ChemistrySelect* **2019**, *4*, 9562–9569. [CrossRef]
114. Wang, S.; Gao, W.; Gao, F.; Dong, J.; Zhang, P.; Chen, G. Enhanced lithium adsorption on an anion- and cation-codoped lithium manganese oxide ion sieve with athin fluoride-protective coating layer. *Ind. Eng. Chem. Res.* **2024**, *63*, 9527–9537. [CrossRef]

Disclaimer/Publisher's Note: The statements, opinions and data contained in all publications are solely those of the individual author(s) and contributor(s) and not of MDPI and/or the editor(s). MDPI and/or the editor(s) disclaim responsibility for any injury to people or property resulting from any ideas, methods, instructions or products referred to in the content.